# Electron Paramagnetic Resonance and Solid-State NMR Study of Cation Distribution in $LiGa_yCo_{1-y}O_2$ and Effects on the Electrochemical Oxidation

**Ekaterina Zhecheva and Radostina Stoyanova**

*Institute of General and Inorganic Chemistry, Bulgarian Academy of Sciences, 1113 Sofia, Bulgaria*

**Ricardo Alcántara and José L. Tirado***

*Laboratorio de Química Inorgánica, Universidad de Córdoba, Edificio C-3, Primera Planta, Campus de Rabanales, 14071 Córdoba, Spain*

*Received: December 23, 2002; In Final Form: March 11, 2003*

$LiGa_yCo_{1-y}O_2$ solid solutions, obtained under a high-pressure (3 GPa), were studied by high-frequency electron paramagnetic resonance (EPR) of $Ni^{3+}$ spin probes and $^{71}Ga$ MAS NMR. $^{71}Ga$ MAS NMR experiments exhibit complex spectra that correspond to octahedral coordination and quadrupolar effects. For Ga-substituted oxides, high-frequency EPR of $Ni^{3+}$ spin probes shows the existence of two new kinds of $Ni^{3+}$ ions in tetragonally elongated octahedra with $g_\perp > g_{||}$. These ions are characterized by slightly different *g*-tensor and temperature of transition from dynamic to static Jahn−Teller effect. The extent of the local tetragonal distortion has been deduced from $g_{||}$. The reinforcement of the tetragonal distortion of $NiO_6$ for $LiGa_yCo_{1-y}O_2$ as compared to $LiCoO_2$ reflects the different structure characteristics of the $Ga_yCo_{1-y}O_2$ and $CoO_2$ layers. For Ga-rich composition, X-band EPR spectra exhibit a new signal with $g \approx 5$ ascribable to high-spin $Ni^{3+}$ located near defect sites. As compared to the Ga-free $LiCoO_2$, a clipping effect in the slabs induced by the Ga inhibits the expansion of the *c* lattice parameter when $LiGa_{0.1}Co_{0.9}O_2$ is oxidized.

## Introduction

Layered $LiCoO_2$ with $R\bar{3}m$ space group is usually the active material of the positive electrode in commercial lithium-ion batteries. By means of partial cobalt substitution by elements such as Al, Ga, Mg, and B, and also by doping and coating, the properties of the pristine $LiCoO_2$ material are changed.[1−8] Thus, small amounts of B or Mg enhance the electrochemical performance. Recently, an increase of the stability upon cycling by coating with $ZrO_2$ has been reported. On the other hand, it has been demonstrated that Al increases the working voltage of $LiAl_yCo_{1-y}O_2$ electrodes in lithium cells. This fact has been interpreted as a result of the participation of oxygen in the redox processes. The modification of the working voltage is of interest for both the theoretical work and the development of a new battery generation. The optimization and development of these cathode materials requires a detailed study of their structural properties. Thus, the distribution of Al in octahedral sites of $LiAl_yCo_{1-y}O_2$ and the effect of Co in the $^{27}Al$ NMR (MAS) spectra have been previously studied.[4] The increase of the voltage for the Ga-substituted $LiCoO_2$ compounds can be even higher than that for the Al-substituted compounds. Unlike $LiAl_yCo_{1-y}O_2$ compounds, $LiGa_yCo_{1-y}O_2$ can be only obtained under high-pressure conditions (3 GPa, 850 °C).[3] It has been found that larger Ga substitutes for smaller Co in the $CoO_2$ layers, the layered structure being preserved up to $y = 0.5$.

In this work, cation distribution in the high-pressure Ga-substituted $LiCoO_2$ compounds is studied by local spectroscopic techniques such as electron paramagnetic resonance (EPR) of $Ni^{3+}$ spin probes and solid-state $^{71}Ga$ and $^{27}Al$ NMR and correlated with the electrochemical behavior. For the sake of comparison, $LiAl_yCo_{1-y}O_2$ and $LiAl_yGa_{1-y}O_2$ compounds have been prepared at high pressure.

## Experimental Section

$LiGa_yCo_{1-y}O_2$ with $y = 0.0$, 0.05, 0.1, 0.25, and 0.5 was obtained at 3 GPa of pressure as described elsewhere.[3] To facilitate the interpretation of solid-state $^{71}Ga$ NMR spectra, $LiAl_yGa_{1-y}O_2$ and $LiAl_yCo_{1-y}O_2$ solid solutions with layered crystal structure were prepared under high pressure as reference materials. $LiAl_yGa_{1-y}O_2$ with $y = 0.2$ and 0.8 was obtained by solid-state reaction between $Li_2O_2$, $Ga_2O_3$, and $Al_2O_3$ at 850 °C under 3 GPa during 7 h. The unit cell parameters are as follows: $a = 2.823\,44(3)$ Å, $c = 14.2715(3)$ Å, and oxygen parameter $z = 0.261\,81(23)$ for $y = 0.20$ and $a = 2.889\,62(3)$ Å, $c = 14.4199(3)$ Å, $z = 0.259\,75(26)$ for $y = 0.8$. $LiAl_yCo_{1-y}O_2$ samples with $y = 0.1$ and 0.9 were prepared by citrate precursor methods as described elsewhere.[4] After that, the samples are annealed at 850 °C under 3 GPa for 1 h. The unit cell parameters of $LiAl_{0.1}Co_{0.9}O_2$ prepared under high and atmospheric pressure are identical. The Al-rich composition with $y = 0.9$ is obtained under high pressure only: $a = 2.800\,88(3)$ Å; $c = 14.2113(3)$ Å; $z = 0.2603(2)$. Comparing the synthesis under high and atmospheric pressure, one may conclude that high pressures favor the formation of $LiAl_yCo_{1-y}O_2$ in the whole concentration range, while at atmospheric pressure the aptitude of $LiCoO_2$ to dissolve Al reaches up to $y = 0.8$. High-pressure synthesis was carried out in a $^1/_2$ in. end-loaded piston cylinder apparatus at the Bayerisches Geoinstitut. The details of high-pressure synthesis are given elsewhere.[3]

Electrochemical experiments were carried out in Swagelok-type cells that are represented as $Li/LiPF_6$(EC:DEC)/$LiGa_yCo_{1-y}O_2$. The electrolyte, supplied by Merck, was 1 M $LiPF_6$

* To whom correspondence should be addressed. E-mail: iq1ticoj@uco.es.

10.1021/jp027807t CCC: $25.00 
Published on Web 04/09/2003

dissolved in ethylene carbonate and diethyl carbonate. Cells were done in an Ar-containing glovebox. Potentiostatic charges/discharges of the cells were performed by changing the voltage 10 mV every 1.0 h in a MacPile II system at room temperature.

Ex situ X-ray diffraction (XRD) patterns of partially charged electrodes were recorded after opening the cells in the drybox and covering the positive electrode with a plastic protective film to avoid exposure to air. For XRD, the instrument was a Siemens D5000 equipped with Cu K$\alpha$ radiation.

EPR measurements at 9.23 GHz (X-band) were carried out in an ERS 220/Q spectrometer within the temperature range 85−410 K. The *g*-factors were established with respect to a $Mn^{2+}$/ZnS standard. The high-frequency EPR spectra were recorded at a single-pass transmission EPR spectrometer built in the High-Magnetic Field Laboratory, Grenoble, France. The frequencies were changed from 95 to 345 GHz using Gunn diodes and their multipliers. The detection of absorption was performed with a bolometer. The recording temperatures were varied from 5 to 300 K using a variable-temperature insert (Oxford Instruments).

NMR MAS of $^{71}Ga$ and $^{27}Al$ were recorded at room temperature in a Bruker ACP400 instrument.

## 3. Results and Discussion

**3.1. Effect of Co Nucleus on the $^{71}Ga$ NMR.** The XRD patterns of all samples studied here were ascribable to the $R\bar{3}m$ space group. Because of the similar scattering of X-rays by Ga and Co, a better understanding of the cation distribution in layered $LiGa_yCo_{1-y}O_2$ compounds was obtained by solid-state NMR and EPR spectroscopic techniques. The $^{71}Ga$ NMR MAS spectra of selected compounds in the $LiGa_yCo_{1-y}O_2$ series are shown in Figure 1A. For comparison, the spectrum of $\gamma$-$LiGaO_2$ is also included in Figure 1B, and selected members of the $LiAl_yGa_{1-y}O_2$ series are shown in Figure 1C. As usually found in oxide and phosphate compounds,[9−11] the NMR solid-state spectra of $^{71}Ga$ with nuclear spin of $I = {}^3/_2$ are complicated by large quadrupolar couplings, leading to line shapes with a large second-order quadrupolar broadening. Even when the coupling constants are not specially large, the MAS spectra become very complicated because of the overlap of the spinning sidebands (SSB).[10] However, it should be noted that the NMR spectra in Figure 1A,C are quite similar for all of the members of each series, irrespective of Ga content. Similar to aluminum in $LiAl_yCo_{1-y}O_2$,[4] an occupancy of Ga in octahedral sites with a central signal at ca. 40 ppm is observed for Ga-substituted compounds, in agreement with the Rietveld refinement previously reported.[3]

Spinning sidebands and quadrupolar effects are also the origin of the complex spectra of $\gamma$-$LiGaO_2$. A larger isotropic chemical shift than that found for both $LiGa_yCo_{1-y}O_2$ and $LiAl_yGa_{1-y}O_2$ is now observed, which is characteristic of tetrahedral Ga. The spectrum is very similar to that described by Massiot et al. for tetrahedral Ga in $GaPO_4$.[10] Concerning Ga environment in $LiAl_yGa_{1-y}O_2$, the spectra in Figure 1C also agree with octahedral coordination with an isotropic chemical shift. However, the component signals occur at a chemical shift range of lower values (ca. 20 ppm) than those for $LiGa_yCo_{1-y}O_2$. The isotropic shifts of each one are expected to be different in each series as affected by Co, similar to that found in $LiAl_yCo_{1-y}O_2$. Cobalt seems to shift downfield the signals of both octahedral Ga and Al.

In Figure 1, it is clear that the complexity of the $^{71}Ga$ spectra is due to quadrupolar effects exclusively and not to the distribution of Co or Al neighbors. This behavior contrasts with the $^{27}Al$ spectra of $LiAl_yCo_{1-y}O_2$, in which a Bernouillian distribution of signals was demonstrated to originate the NMR spectra.[4] Hence, $^{71}Ga$ NMR seems to be less sensitive to these distributions than $^{27}Al$ or the resolution is complicated by the quadrupolar effects or both.

Figure 2 shows that the $^{27}Al$ MAS NMR spectra of $LiAl_yGa_{1-y}O_2$ are also broadened by quadrupolar effects and not by the distribution of neighbors. Finally, the $^{27}Al$ NMR spectra of selected $LiAl_yCo_{1-y}O_2$ samples obtained at 3 GPa allow discernment of different environments, which are included in the broad central signal (Figure 2), as in previous $LiAl_yCo_{1-y}O_2$ samples obtained at atmospheric pressure,[4] In summary, the cationic environments, that is, $Co^{3+}$, $Ga^{3+}$, and $Al^{3+}$, in these layered compounds are always octahedral. The presence of cobalt neighbors in the lattice has great effect in the $^{27}Al$ NMR spectra, irrespective of the preparation condition. A less marked effect of cobalt is comparatively seen in the $^{71}Ga$ NMR spectra.

**3.2. Effect of Ga on the EPR Spectrum of $Ni^{3+}$ Spin Probes in $LiGa_yCo_{1-y}O_2$.** The increase in the mean M−O bond length (from 1.932 to 1.970 Å)[3] caused by the larger $Ga^{3+}$ would lead to a weakness of the crystal field of $Co^{3+}$ in $LiGa_yCo_{1-y}O_2$. However, $Co^{3+}$ remains in a low-spin configuration as was shown by electron paramagnetic resonance. The diamagnetic character of the $LiGa_yCo_{1-y}O_2$ matrix permits one to explore the effect of the nontransition metal ions on the transition metal ions by EPR of $Ni^{3+}$ spin probes.

Nickel is found to replace $Co^{3+}$ ions from the $CoO_2$ layers, thus forming $LiNi_xCo_{1-x}O_2$ solid solutions in the whole concentration range $0 \leq x \leq 1$.[12,13] Because of the high sensitivity of the EPR spectroscopy in the X-band, even small amounts of paramagnetic $Ni^{3+}$ ions replacing $Co^{3+}$ in the diamagnetic $LiGa_yCo_{1-y}O_2$ can be detected by EPR (less than 0.05%, which is the common impurity content for cobalt salts without special purification). In the $CoO_2$ layers, the $Ni^{3+}$ spin probes adopt the low-spin configuration with a double degenerate ground state, which is Jahn−Teller unstable in a trigonal symmetry. Therefore, the EPR spectrum of $Ni^{3+}$ is dominated by the Jahn−Teller effect.[14−16]

The X-band EPR spectra of $Ni^{3+}$ spin probes in pure $LiCoO_2$ and $LiGa_yCo_{1-y}O_2$ are compared in Figure 3. Above 100 K, the EPR spectrum of $Ni^{3+}$ spin probes in $LiCoO_2$ consists of a single line with a Lorentzian shape and $g = 2.142$ due to the dynamic Jahn−Teller effect. When $Ga^{3+}$ replaces $Co^{3+}$ in $LiGa_yCo_{1-y}O_2$, there is a strong change in the EPR profile of $Ni^{3+}$ spin probes. A tetragonally asymmetric signal with $g_\perp = 2.1925$ and $g_{||} = 2.0422$ is superimposed on the Lorentzian line, the intensity of the latter decreasing with the Ga content. In the EPR notation, the tetragonal signal corresponds to a tetragonally elongated "static" Jahn−Teller configuration. For Ga-rich compositions, a new signal with an effective $g \approx 5$ grows in intensity. This can be tentatively assigned to $Ni^{3+}$ in a high-spin configuration. Because a switch from low- to high-spin $Ni^{3+}$ in the dense oxygen packing of layered $LiMO_2$ is improbable, the high-spin $Ni^{3+}$ probes have to be associated with defect crystal sites. However, these defects are specific for the Ga-substituted oxides.

Below 60 K, the EPR profile of $Ni^{3+}$ undergoes a strong change: the single line is broken into several signals. The temperature of splitting of the single line depends on whether Ga or Co/Ga participates in the crystal host. Figure 4 gives the EPR spectra of $Ni^{3+}$ recorded at 9.23 and 115 GHz. The use of high-frequency (HF) EPR permits more precise differentiation between the $Ni^{3+}$ ions having slightly different *g*-values. However, due to the lower sensitivity of HF-EPR technique

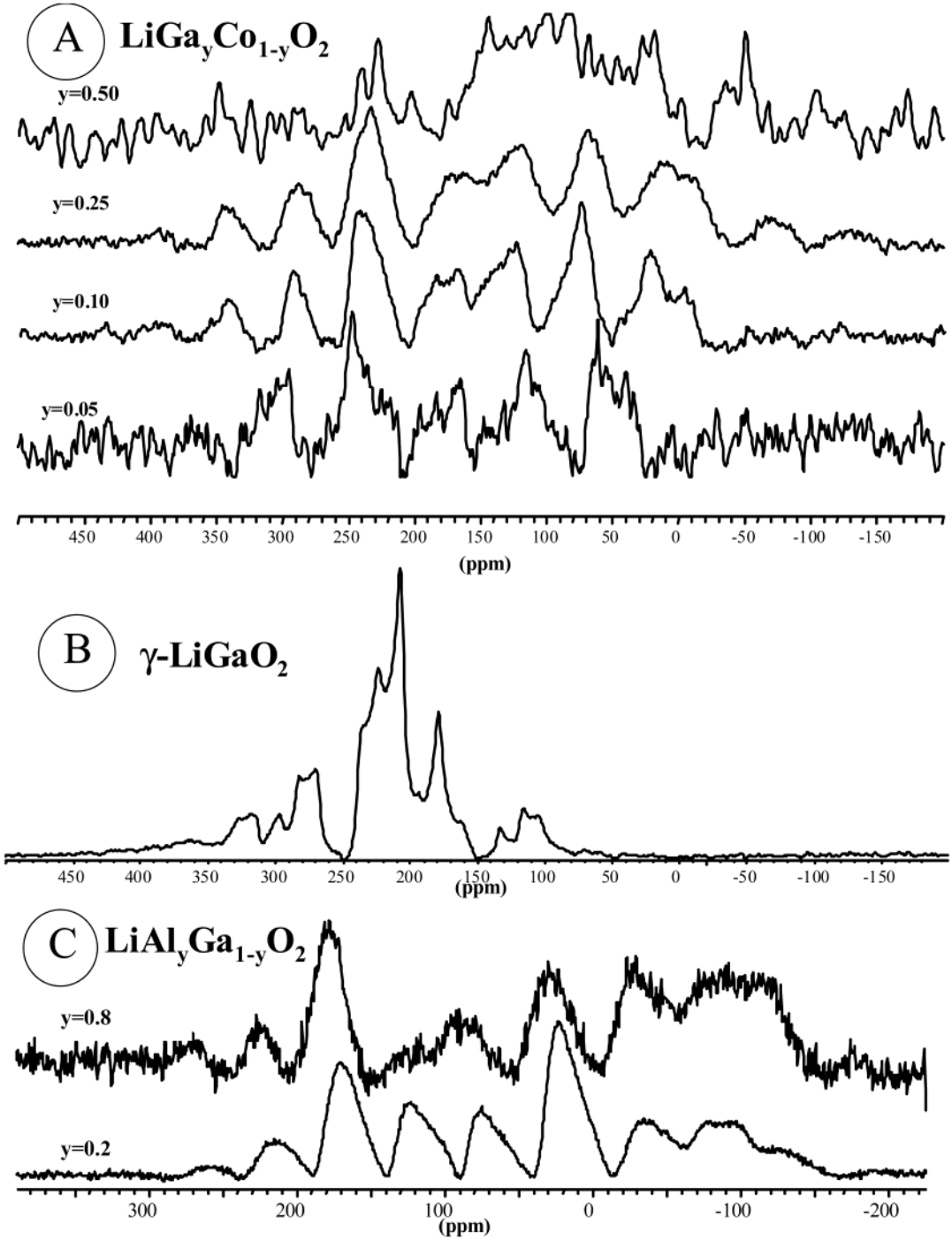


**Figure 1.** $^{71}$Ga NMR MAS spectra of (A) $LiGa_yCo_{1-y}O_2$ and (B) $\gamma$-$LiGaO_2$ compounds for $y = 0.05$, 0.1, 0.25, and 0.5 with spin rate = 5.5 kHz and (C) $LiAl_yGa_{1-y}O_2$ compounds with $y = 0.20$ and 0.8 and spin rate = 6 kHz.

(single-pass technique) as compared to the conventional X-band EPR spectrometer, a higher spin concentration is needed. That is why the oxides have additionally been doped with Ni with a concentration of Ni/(Co+Ga) = 0.006. In this case, the signal in the X-band EPR spectrum is slightly broadened, but the EPR profile is preserved. Moreover, the crystal structure parameters of Ni-doped $LiGa_yCo_{1-y}O_2$ remain the same.

At 5 K, the EPR spectrum of $Ni^{3+}$ in pure $LiCoO_2$ consists of an anisotropic doublet and a nearly symmetric single line in the central part. This feature is typical for $^2E_g$ ions with a weak to moderate Jahn−Teller coupling (intermediate Jahn−Teller effect).[17−19] According to our previous X- and Q-band EPR studies on Ni-doped $LiCoO_2$,[14] the anisotropic doublets originate from the ground vibronic doublet state, while the single line can be assigned to an excited vibronic singlet or relaxation-averaged singlet. The corresponding $g$-factors are

$$g_+ = g_1 + qg_2f(\bar{\alpha})$$

$$g_- = g_1 - qg_2f(\bar{\alpha})$$

Here, $q$ is the vibronic reduction factors, $f(\bar{\alpha})$ is the function of the mean angle, $\bar{\alpha}$, between the vectors of the random strains and the external magnetic field, and $g_2 = g_1 - 2.0023$ is the contribution of the orbital magnetic moment to the overall magnetic moment.

In addition, a signal with a tetragonal symmetry can also be resolved in the EPR spectrum of $Ni^{3+}$ ions in $LiCoO_2$ (Figure

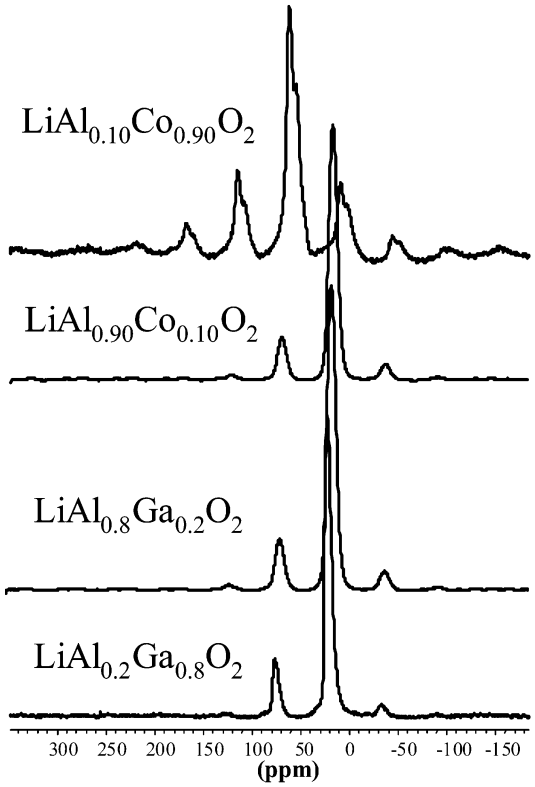


**Figure 2.** $^{27}Al$ NMR MAS spectra with spin rate = 5.5 kHz of $LiAl_{0.1}Co_{0.9}O_2$, $LiAl_{0.9}Co_{0.1}O_2$, $LiAl_{0.8}Ga_{0.2}O_2$, and $LiAl_{0.2}Ga_{0.8}O_2$ obtained at 3 GPa and heated at 850 °C.

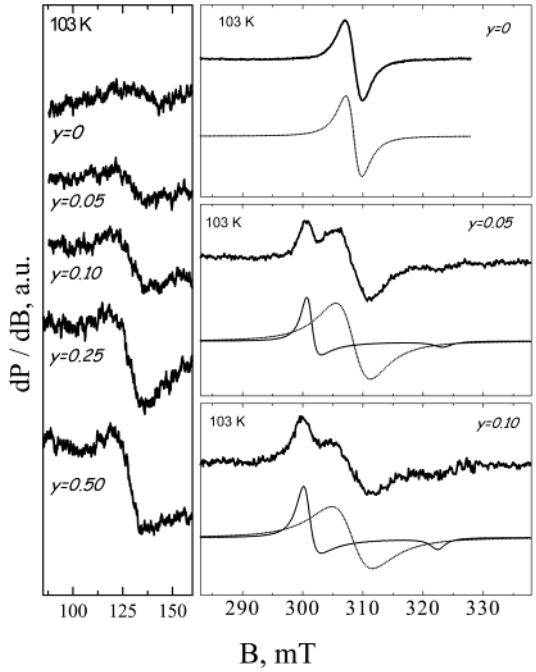


**Figure 3.** X-band EPR spectra at 103 K of $Ni^{3+}$ spin probes in $LiGa_yCo_{1-y}O_2$. The experimental spectrum (full lines) and the simulated axially symmetric and Lorentzian signals (dotted and dashed lines) are shown.

4). This feature is characteristic of the "quasistatic" Jahn−Teller effect: random strengths permit coupling of the excited $A_1$-($A_2$) vibronic levels to the ground vibronic doublet state, thus leading to a new set of vibronic basis states the vibrational parts of which represent a distortion along one of the cubic 4-fold axes. The transition from intermediate to quasistatic Jahn−Teller effect is usually associated with an increased ratio of the random strains in the crystal host as compared to the strengths of the Jahn−Teller coupling.

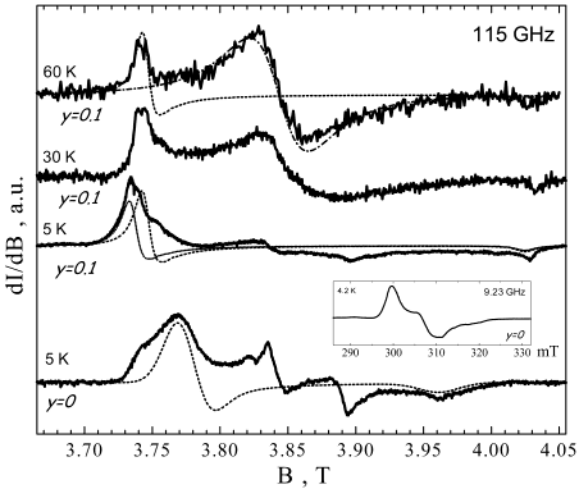


**Figure 4.** Temperature evolution of EPR spectra at 115 GHz for $Ni^{3+}$ spin probes in $LiCoO_2$ and $LiGa_{0.1}Co_{0.9}O_2$ ($y = 0.1$). The inset shows the EPR spectrum at 9.23 GHz (X-band) of $Ni^{3+}$ in $LiCoO_2$. Experimental and simulated spectra are given.

For Ga-substituted oxides, the EPR spectrum at 60 K displays two signals: a tetragonally symmetric signal and a second asymmetric line. The tetragonal signal possesses EPR parameters identical with that for the signal observed in the X-band EPR spectrum at 103 K. Below 60 K, a new tetragonally symmetric signal with $g_\perp = 2.1994$ and $g_\parallel = 2.0414$ is developed from the single line. The values of the $g$-tensor for the low-temperature tetragonal signal differ from that in $LiCoO_2$ (Table 1). In addition, the signal due to $Ni^{3+}$ with a moderate Jahn−Teller effect is barely visible for $LiGa_yCo_{1-y}O_2$ at 5 K. The $g$-value of this signal remains nearly unchanged as compared to the pure $LiCoO_2$.

Summarizing, one may conclude that the two configurations detected for $Ni^{3+}$ spin probes in $LiGa_yCo_{1-y}O_2$ do not match the distortion of the lattice site in the trigonal $LiCoO_2$ host. However, it appears that the mean $\bar{g}$-value, $\bar{g} = (2g_\perp + g_\parallel)/3$, correlates with the mean Co(Ga)−O bond length determined from the Rietveld analysis of the XRD diffraction lines (Table 1), thus indicating location of these ions in host layers. The appearance of tetragonal $Ni^{3+}$ ions in the trigonal $LiCoO_2$ host can be understood in terms of a local tetragonal distortion not affecting the collective trigonal symmetry. A local tetragonal distortion of the $NiO_6$ octahedron due to the Jahn−Teller effect has been established by means of Ni−K edge extended X-ray absorption fine structure (EXAFS) and X-ray absorption near-edge structure (XANES) in layered $LiNi_xCo_{1-x}O_2$ oxides.[20,21] An important feature is the weaker tetragonal distortion for $NiO_6$ in $LiNi_xCo_{1-x}O_2$ as compared to that for $NaNiO_2$ in which a collective tetragonal deformation takes place.

The higher value of $g_\perp$ as compared to $g_\parallel$ indicates that $Ni^{3+}$ is in a tetragonally elongated octahedron with a $^2A_{1g}$ ground state. The values of $g_\perp$ and $g_\parallel$ can be expressed by [22]

$$g_\perp = g_e + 2(\xi/\delta)^2 + 3\xi(1.38/E_3 + 0.62/E_4)$$

$$g_\parallel = g_e + 2(\xi/\delta)^2$$

The deviation of the $g_\parallel$ value from the value of the free electron ($g_e$) results from the doublet-quartet energy separation, $\delta$, while doublet-quartet energy separation and ligand-field energies of the transitions $^2A_{1g} \rightarrow {}^2{}_aT_{2g}$, $^2{}_bT_{2g}$ ($E_3$, $E_4$) contribute to the $g_\perp$-

**TABLE 1: *g*-Tensor for Low-spin $Ni^{3+}$ in $LiGa_yCo_{1-y}O_2$ Host, the Mean M−O Bond Length, and the Extent of Tetragonal Distortion Expressed by the Ratio between Two Long and Four Short Bond Lengths ($r_{ax}/r_{eq}$)**

| matrix | $g_\perp$ | $g_{\|\|}$ | $\bar{g}$ | $g_1$ | $qg_2$ | $r_{av}$, Å | $r_{ax}/r_{eq}$ |
|---|---|---|---|---|---|---|---|
| | | | Matrix with Trigonal Symmetry | | | | |
| $LiCoO_2$ | 2.1759 | 2.0739 | 2.1419 | 2.1415 | 0.0333 | 1.932[3] | |
| $LiCo_{0.9}Ga_{0.1}O_2$ | 2.1925 | 2.0422 | 2.1424 | | | 1.940[3] | |
| | 2.1994 | 2.0414 | 2.1467 | | | | |
| | | | Matrix with Tetragonal Symmetry | | | | |
| $LaSrGa_{0.93}Ni_{0.07}O_4$[23] | 2.227 | 2.044 | 2.166 | | | 1.99 | 1.07 |
| | 2.250 | 2.044 | 2.181 | | | | |
| $NaNiO_2$[24] | 2.283 | 2.030 | 2.199 | | | 1.99 | 1.12 |
| $La_2Li_{0.5}Ni_{0.5}O_4$[23] | 2.256 | 2.014 | 2.174 | | | 1.95 | 1.20[25] |

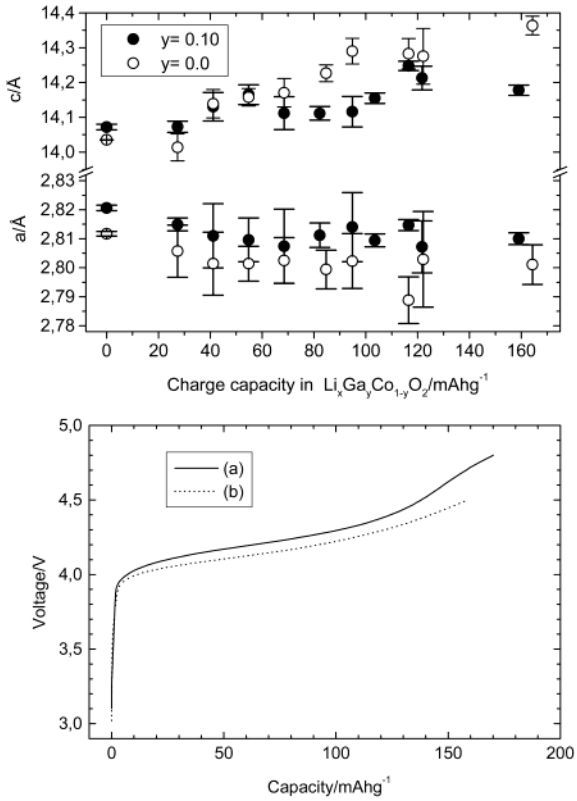


**Figure 5.** Change in *a* and *c* hexagonal lattice parameters (top) and voltage vs capacity curves (bottom) for (a) $LiGa_{0.1}Co_{0.9}O_2$ and (b) $LiCoO_2$ in lithium cells. Both samples were obtained at 3 GPa.

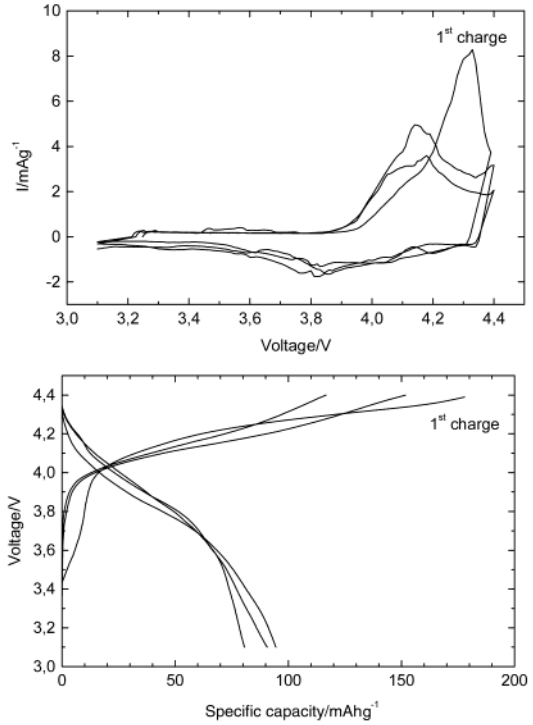


**Figure 6.** Potentiostatic charge/discharge cycles in lithium cells of $LiAl_{0.10}Co_{0.90}O_2$ obtained 3 GPa. Scan rate = 10 mV/h.

value, and $\xi$ is the effective spin−orbit coupling parameter. In terms of Jahn−Teller stabilization, the low-spin configuration (the doublet state) can lower its energy with respect to the high-spin configuration (quartet state) by increasing the tetragonal distortion. This will result in a $g_{||}$-value approaching $g_e$. Table 1 gives the available experimental data of the *g*-tensor of $Ni^{3+}$ in tetragonally distorted crystal lattices (such as $La_2Li_{0.5}Ni_{0.5}O_4$ and $LaSrGaO_4$) with a $K_2NiF_4$-type structure and monoclinic layered $NaNiO_2$.[23,24] This experimentally obtained relation makes it possible to deduce roughly the extent of tetragonal distortion of $NiO_6$ in Ga-substituted $LiCoO_2$. It appears that the extent of the local tetragonal distortion for the $Ni^{3+}O_6$ octahedron is stronger with $LiGa_yCo_{1-y}O_2$ as compared to $LiCoO_2$ and reaches about $r_{ax}/r_{eq} \geq 1.08$. This value is lower than that for $NaNiO_2$ and comparable with that found in $LiNiO_2$: $r_{ax}/r_{eq} = 1.09$. The reinforcement of the tetragonal distortion of $NiO_6$ for $LiGa_yCo_{1-y}O_2$ as compared to $LiCoO_2$ reflects the different structure characteristics of the $Ga_yCo_{1-y}O_2$ and $CoO_2$ layers and would be of importance for lithium deintercalation.

**3.3. Effect of Ga on the Lithium Deintercalation from $LiGa_yCo_{1-y}O_2$.** On the other hand, the Co substitution by Ga leads to changes in the electrochemical behavior of the layered $LiCoO_2$.[3] To explore this effect, we have studied the charge/discharge of $LiCoO_2$ and $LiGa_{0.1}Co_{0.9}O_2$ high-pressure samples as positive electrodes in lithium cells (Figure 5). For comparison, the electrochemical behavior in of $LiAl_{0.10}Co_{0.90}O_2$ obtained at 3 GPa is also shown in Figure 6, in which a behavior similar to that previously reported for Al-containing samples obtained at atmospheric pressure is exhibited.[26] By ex situ XRD patterns of partially charged electrodes, it is observed that the variations of the cell parameters (significant expansion of *c* and slight contraction of *a*) are smaller for the sample that contains Ga ($y = 0.1$) as compared to those for the Ga-free sample ($y = 0$). An equivalent behavior was previously observed in the $LiAl_yCo_{1-y}O_2$ system.[5] In addition, the electrochemical oxidation in lithium cells takes place in higher voltage for the Ga-containing sample. The higher lattice expansion along *c* found for $y = 0.0$ as compared to $y = 0.1$ can be correlated with the increase in intensity of the high-spin $Ni^{3+}$ EPR signal ($g = 5$) with Ga content, previously described. Thus, gallium (and probably aluminum) atoms induce an increased number of defect sites that could be concentrated, for example, as interlayer $Ni^{3+}$ in grain boundaries. Such defects may cause a clipping effect on the slabs that avoids a more marked expansion.

On the other hand, the presence of Ga in the Co−Ga−O system decreases the reversible capacity even more that in the case of the Al-containing sample (Figures 5 and 6). An

improvement of the capacity retention is not observed with Ga. Hence, both the clipping effect induced by Ga and the tetragonal distorted $NiO_6$ octahedra may deteriorate the reversible capacity of the material to adapt its microstructure to the lithium extraction by electrochemical process. Moreover, lithium ordering is suppressed by this mechanism, as shown in Figure 5 and ref 3.

## Conclusions

Occupancy of gallium in octahedral sites of layered $LiGa_yCo_{1-y}O_2$ obtained at 3 GPa is detected by using $^{71}Ga$ MAS NMR spectroscopy. The $^{71}Ga$ chemical shift varies with Co content, and the spectra evidence a large quadrupolar coupling.

The EPR spectra of $Ni^{3+}$ probes in the series show a reinforcement of local tetragonal distortion of $NiO_6$ octahedra in the trigonal $LiGa_yCo_{1-y}O_2$ as compared to that in $LiCoO_2$. On increase of the gallium content, the EPR spectra of layered $LiGa_yCo_{1-y}O_2$ show the occurrence of $Ni^{3+}$ probes in a high-spin configuration associated with defect crystal sites.

The differences between the microstructure of $LiGa_yCo_{1-y}O_2$ and $LiCoO_2$ affect the electrochemical behavior: the operation voltage increases and the reversible capacity decreases on increase of Ga content. Finally the *c* expansion on lithium extraction is less marked in Ga-containing samples because of the clipping effect of defect crystal sites.

**Acknowledgment.** The authors acknowledge financial support from MCyT (Contract MAT2002-00434) and Programa Ramón y Cajal. R.S. is grateful to the EC for a grant of an EU "IHP − Access to Research Infrastructures" Program (Contract No. HPRI-1999-CT-0004 to D.C. Rubie) to perform high-pressure synthesis experiments at the Bayrisches Geoinstitut, Universität Bayreuth, Bayreuth, Germany. The high-frequency EPR measurements (GHz) carried out at High Magnetic Field Laboraty in Grenoble, France, were supported by European Community "Access to Research Infrastructure action of the Improving Human Potential Program". The authors are very grateful to Dr. G. Bromiley and Dr. T. Boffa Ballaran from Bayerisches Geoinstitut and Dr. A.-L. Barra from High Magnetic Field Laboratory in Grenoble for their help.

## References and Notes

(1) Alcántara, R.; Lavela, P.; Tirado, J. L.; Zhecheva, E.; Stoyanova, R. *J. Solid State Electrochem.* **1999**, *3*, 121.

(2) Ceder, G.; Chiang, Y.-M.; Sadoway, D. R.; Aydinol, M. K.; Jang, Y. I.; Huang, B. *Nature* **1998**, *392*, 694.

(3) Stoyanova, R.; Zhecheva, E.; Bromiley, G.; Ballaran, T. B.; Alcántara, R.; Corredor, J. I.; Tirado, J. L. *J. Mater. Chem.* **2002**, *12*, 2501.

(4) Gaudin, E.; Taulelle, F.; Stoyanova, R.; Zhecheva, E.; Alcántara, R.; Lavela, P.; Tirado, J. L. *J. Phys. Chem. B* **2001**, *105*, 8081.

(5) Jang, Y. I.; Huang, B.; Wang, H.; Sadoway, D.; Ceder, G.; Chiang, Y. M.; Liu, H.; Tamura, H. *J. Electrochem. Soc.* **1999**, *146*, 862.

(6) Mladenov, M.; Stoyanova, R.; Zhecheva, E.; Vassilev, S. *Electrochem. Commun.* **2001**, *3*, 410.

(7) Cho, J.; Kim, Y. J.; Kim, T. J.; Park, B. *Angew. Chem., Int. Ed.* **2001**, *40*, 3367.

(8) Chen, Z.; Dahn, J. *Electrochem. Solid State Lett.* **2002**, *5*, A213.

(9) Massiot, D.; Revel, R.; Magnenet, C.; Bazin, D. *Solid State Nucl. Magn. Reson.* **2000**, *16*, 103.

(10) Massiot, D.; Vosegaard, T.; Magneron, N.; Trumeau, D.; Montouillout, V.; Berthet, P.; Loiseau, T.; Bujoli, B. *Solid State Nucl. Magn. Reson.* **1999**, *15*, 159.

(11) Massiot, D.; Montouillout, V.; Fayon, F.; Florian, P.; Bessada, C. *Chem. Phys. Lett.* **1997**, *272*, 295.

(12) Delmas, C.; Saadoune, I.; *Solid State Ionics* **1992**, *53*−*56*, 370.

(13) Zhecheva, E.; Stoyanova, R. *Solid State Ionics* **1993**, *66*, 143.

(14) Angelov, S.; Friebel, C.; Zhecheva, E.; Stoyanova, R. *J. Phys. Chem. Solids* **1992**, *53*, 443.

(15) Stoyanova, R.; Zhecheva, E.; Friebel, C. *J. Phys. Chem. Solids* **1993**, *54*, 9.

(16) Stoyanova, R.; Zhecheva, E.; Alcántara, R.; Lavela, P.; Tirado, J. L. *Solid State Commun.* **1997**, *102*, 457.

(17) Ham, F. S. *Phys. Rev.* **1968**, *166*, 307.

(18) Reynolds, R. W.; Boatner, L. A. *Phys. Rev. B* **1975**, *12*, 4735.

(19) Setser, G. G.; Estle, T. L. *Phys. Rev. B* **1978**, *17*, 4735.

(20) Rougier, A.; Delmas, C.; Chadwick, A. V. *Solid State Commun.* **1995**, *94*, 123.

(21) Nakai, I.; Takahashi, K.; Shiraishi, Y.; Nakagome, T.; Nishikawa, F. *J. Solid State Chem.* **1998**, *140*, 145.

(22) Lacroix, R.; Hoechli, U.; Mueller, K. A. *Helv. Phys. Acta* **1964**, *37*, 627.

(23) Reinen, D.; Kesper, U.; Belder, D. *J. Solid State Chem.* **1995**, *116*, 355.

(24) Chappel, E.; Núñez-Regueiro, M. D.; Chouteau, G.; Isnard, O.; Darie, C. *Eur. Phys. J. B* **2000**, *17*, 615.

(25) Abou-Waeda, S.; Pietzuch, W.; Berghöfer, G.; Kesper, U.; Messa, W.; Reinen, D. *J. Solid State Chem.* **1998**, *138*, 18.

(26) Alcántara, R.; Lavela, P.; Relaño, P. L.; Tirado, J. L.; Zhecheva, E.; Stoyanova, R. *Inorg. Chem.* **1998**, *37*, 264.